

Aeroacoustics wind noise optimization for vehicle's side mirror base

Moath N. Zaareer^a, Abdel-Hamid Ismail Mourad^{a,c,d,*}, Tariq Darabseh^b, Kassim Abdullah^a, Mostafa S.A. ElSayed^{a,e}

^a Mechanical and Aerospace Engineering Department, College of Engineering, United Arab Emirates University, Al-Ain, P.O. BOX 15551, United Arab Emirates

^b Aeronautical Engineering Department, Jordan University of Science and Technology, P.O. Box 3030, Irbid 22110, Jordan

^c National Water and Energy Center, United Arab Emirates University, Al Ain, P.O. Box-15551, United Arab Emirates

^d On leave from Mechanical Design Department, Faculty of Engineering, Helwan University, Cairo, Egypt

^e Department of Mechanical and Aerospace Engineering, Carleton University, Ottawa, ON K1S 5B6, Canada

ARTICLE INFO

Keywords:

Aeroacoustics
Aerodynamic forces
ANSYS
CFD
Side mirror

ABSTRACT

Extreme effect of noise pollution includes deafness and mental breakdown and in main cities automobiles are a main source of noise. The literature concentrates on the side mirror part and lacks analysis on mirror base (arm) that connects the mirror part to the vehicle's body. This work focuses on lowering noise emission from vehicles by optimizing the orientation of the mirror base. In this manuscript, the connection between the mirror and its base is set as a vertical rotational axis, and multiple angles are examined to determine the optimal angle for the mirror base ranging from 0 to 90°. The Scale Adaptive Simulation (SAS) model is utilized for the simulation combined with Ffowcs-Williams and Hawkings as the acoustics model. The simulation is conducted using ANSYS Computational Fluid Dynamics to analyse the real case. The results show that, the optimal orientation of the mirror's base is ~85° relative to the horizontal axis, as it yields minor acoustic noise and relatively the best aerodynamic force performance. The difference in changing the mirror base orientation results up to 32 dB difference in sound pressure level.

1. Introduction

Cities are full of economic opportunities and business activities. However, this development of transport and industry results in high noise levels, and citizens suffer from noise pollution. Noise pollution causes problems ranging from communication interference and insomnia to deafness and mental breakdown, and for sensitive people could affect memory and raise blood pressure [1]. The citizens need to be educated about noise pollution and the possible effects [2,3], as it could result in preventive measures taken. For example, citizens could wear noise-cancelling headphones, or ear guards. Furthermore, government interference is required by setting regulations on vehicle noise and working time of construction. Recognizing this as a prime issue, the European parliament related to the assessment of noise pollution embraced new rules demanding major cities establish a noise

management policy [4,5]. Furthermore, the government of some countries such as Turkey planted trees between the roads to reduce pollution and noise [6]. Although noise is becoming more and more of a problem, it is unnoticed as pollution.

Automobiles are a significant source of noise pollution, affecting both the occupants and pedestrians [7]. A scale of items emitting sound pressure level (SPL) measured in decibels (dB) is shown in Fig. 1. The value of 80 dB and above is considered unpleasant and could cause injuries when listening to for long time. Vehicles are usually in the 70 dB range while in city speeds. However, at highway speeds the noise could reach up to 100 dB [7]. Therefore, the noise generation of the vehicle must be reduced by changing the exterior shape and improving aeroacoustics and possible aerodynamic design, for the comfort of the occupants and surrounding pedestrians.

Aeroacoustics is the study of acoustics generated from air interacting

Abbreviations: BL, Boundary Layer; Cd, Drag Coefficient; CFD, Computational Fluid Dynamics; Cl, Lift Coefficient; dB, decibels; DES, Detached Eddy Simulation; FW-H, Ffowcs-Williams and Hawkings; LES, Large Eddy Simulation; RMS, Root Mean Square; SAE, Society of Automotive Engineers; SAS, Scale Adaptive Simulation; SPL, Sound Pressure Level; TBL, Turbulent Boundary Layer; TKE, Turbulent Kinetic Energy; URANS, Unsteady Reynolds Averaged Navier Stokes; SIMPLE, Semi Implicit Method for Pressure Linked Equations; PISO, Pressure Implicit with Splitting of Operators; SA, Spalart-Allmaras; CAD, Computer Aided Design; CPU, Central Processing Unit.

* Corresponding author.

E-mail address: ahmourad@uaeu.ac.ae (A.-H.I. Mourad).

<https://doi.org/10.1016/j.ijft.2023.100332>

Available online 13 March 2023

2666-2027/© 2023 The Author(s). Published by Elsevier Ltd. This is an open access article under the CC BY-NC-ND license (<http://creativecommons.org/licenses/by-nd/4.0/>).

with an object, as laminar airflow hitting an object turns it turbulent with vortices of air. The vortices create fluctuating pressure area that causes nearby objects to vibrate, thus generating noise. Noise is also generated from the airflow vortices and is transmitted through different paths/regions of the structure; it could travel through leaks in sealings and openings. Although vehicles have sound absorption packages to reduce interior sound, they can only handle a range of frequencies or amplitude, and they are heavy to add freely to a vehicle. The main contributors to the driver's noise hearing are the A-pillar and side mirrors which are closest to the driver [8]. The turbulent wake structure generated from the A-pillar and side mirrors creates a fluctuating pressure zone that vibrates the surrounding structure (vehicle windows) creating noise very close to the driver's ears which affects the ride's quality and comfort. Even though the wheels generate loud noise levels, it is far away from the passengers in most vehicle designs, which negates the effect [9].

In order for noise inside the vehicle to be generated from the exterior of the vehicle, airflow passes through two stages. Firstly, the turbulent airflow creates pressure fluctuations outside the vehicle. Secondly, the difference in pressure causes the vehicle's body to vibrate thus generating noise inside the vehicle. This process is modelled and called Aerovibro-acoustics. Vibroacoustic is the study of vibration and sound combined to influence physiology. The turbulent flow outside the vehicle consists of acoustic pressure and a convective component. The acoustic pressure component relates to acoustic waves travelling and being generated within the flow before reaching the vehicle's structure. The convective component focuses on the pressure regions created by eddies travelling at the convection speed. Both components carry energy transmitted into the vehicle's interior, creating cabin noise that affects the ride quality.

A Corrected Force Analysis Technique (CFAT) was used to study both the hydrodynamic and acoustic pressure on the front side vehicle window shows that the acoustic pressure, although smaller than hydrodynamic pressure (pseudo-sound), still contributes more to interior sound pressure [10]. As the hydrodynamic pressure on the front side window is not correlated with the interior sound field [11]. The acoustic pressure is the prominent contribution to the internal sound pressure. When comparing the effects of hydrodynamic and acoustic pressure inside the car the acoustic pressure governs the hydrodynamic pressure till 2 kHz [12]. Noise coefficient is governed by the threshold, as values coefficients above the threshold corresponding to the pseudo-sound or hydrodynamic part of the signal and those having magnitude lower than the threshold, corresponding to the sound, that is, to the acoustic part of the signal [13,14].

The noise that reaches the occupants' ears is caused by turbulent airflow, and there are several main principles involved in wind noise generation [15]. Although there are five ways in which noise is generated and transmitted in vehicles, we will focus on only four:

Firstly, the pressure fluctuation phenomenon on the side glass. Turbulent airflow outside the vehicle generates a fluctuating surface pressure field on the side glass, including convective and acoustic components. Although the acoustic component is relatively small compared to the convective component, it plays a significant role in the coincidence frequency of the side glass.

Secondly, the pressure fluctuation phenomenon occurring at the mirror. The pressure is highest in the front of the side mirror, where the

flow is steady, as opposed to the rear, where the flow is highly fluctuating. Turbulences at the rear face of the mirror create acoustic waves that move towards the side glass and are likely transmitted inside the vehicle to the driver's ear.

Thirdly, the pressure fluctuation phenomenon on the A-pillar. The A-pillar follows a similar principle to the mirror, where acoustic waves travel to the side glass and are transmitted to the driver's ear inside the vehicle [15].

Lastly, the acoustic sources formed within eddies. Eddies within the turbulent flow can also generate noise and thus constitute acoustic sources. These sources act as quadrupole acoustic sources and are in the vicinity of the side glass, but are considered negligible at automobile speeds.

The study of aerodynamic noise has revealed the significant impact of pressure excitation on the front side window [16]. A wavenumber-spectrum model of the hydrodynamic pressure on the front side window was used to calculate the interior noise, and the model was further enhanced by incorporating the contribution of acoustic pressure to the interior noise [17]. Bremner et al. [18] reviewed the problem of flow-induced sound and vibration in automotive aerodynamic noise, considering the difference between hydrodynamic and acoustic pressure [18,19].

In another study, Alam et al. [20] investigated the sensitivity of pressure on a vehicle's frontal surface to the variation of Reynolds number, yaw angle, and windshield geometry for a group of road vehicles. The results showed that the dimensionless pressure on the side window hardly changes with varying Reynolds numbers, while changing the yaw angles and geometry parameters causes significant changes.

Aerodynamics and aeroacoustics are subjects of considerable interest due to their widespread applications in various fields of engineering and science. Several articles discuss the improvement of acoustics, such as the design requirements for porous materials [21–23]. Reducing interior noise is a major concern in the automotive and aeronautics industries to create quieter cabin environments.

An experimental study about the turbulent wake generated by a vertical sharp-edged flat plate suspended in a shallow channel flow, with and without a gap flow, was conducted [24]. Although the acoustic pressure magnitude is smaller than the hydrodynamic pressure, it contributes significantly more to the internal sound pressure [10]. Previous research has concluded a very satisfactory similarity between simulation and real-life experimental results [25], proving that simulation models can accurately predict fluid behaviour. Several articles demonstrate that accurate numerical analysis can be performed in software that models an experimental wind tunnel, and the best settings have been determined for the most accurate steady-state simulation. Wind tunnel observations, using scaled-down models or numerical simulations, can study virtually everything, including the effect of terrain on wind turbine performance [26,27].

This manuscript employs ANSYS Fluent software to simulate real-world processes, utilizing different turbulence models depending on the specific case being studied. Popular models for transient flow include Large Eddy Simulation (LES) and Detached Eddy Simulation (DES), a hybrid model that combines LES and Reynolds Average Navier Stokes (RANS). A comparison of DES, Spalart-Allmaras, and LES models was conducted, with varying grid resolutions [28–30]. The study concluded that the DES and Spalart-Allmaras combination is not an accurate choice

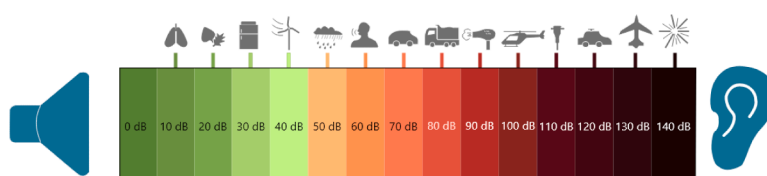


Fig. 1. Noise scale showing different sources sound pressure level in dB.

for determining pressure fluctuations. Advection schemes, such as second-order upwind or second-order hybrid schemes, had no significant influence on downstream pressure fluctuations, and the use of upwind schemes was found to be dissipative. In summary, the DES-SA combination with upwind schemes is not suitable for resolving pressure fluctuations accurately, while advection schemes such as second-order upwind or second-order hybrid schemes had no significant influence on downstream pressure fluctuations, as long as the DES-SA model is avoided.

The aeroacoustic flow sources over the side-view mirror have been predicted, followed by predicting the sound generated from these sources [31,32]. The experiment determines both the Hydrodynamic Pressure Fluctuations on the plate holding the mirror [31] and the sound radiated from the side mirror [32]. Another study measured the accuracy of Unsteady Reynolds Averaged Navier Stokes (URANS) and DES in predicting physics-based noise generation. The results indicated that URANS exaggerates the results and overestimates the structure contribution, while DES simulations can predict the higher frequency sources with fair accuracy [33].

For steady-state flows, the most popular model that outputs accurate results is the K-Omega turbulence model. The K-Omega SST turbulence model [34,35] shows excellent performance in typical aerodynamic flows and has gained popularity in the aeronautical community. It focuses on predicting adverse pressure gradient flows, where other models may fail. However, the K-Omega model is sensitive to free-stream turbulence, streamline curvature, and system rotation, which can produce harmful effects [36].

Research on the shape of the side-view mirror is relevant to this work since the mirror is shaped as a cuboid. Studies have shown that different aspect ratios of a cuboid affect the emitted noise. Aspect ratios smaller than unity result in the reattachment of separated flow, while a larger aspect ratio forms vortices near the trailing edge [37]. Other shapes have also been investigated in terms of aerodynamics or aeroacoustics, such as the flow around a hemisphere [38] and aerodynamic sound reduction for a square cylinder using a pair of cowl plates [39]. The work done on different shapes in the literature helps in predicting the behaviour of the mirror's acoustics and aerodynamic forces.

A simulation of flow around a cube affected by the elevated height reveals that the radiated sound in the vertical direction increases quickly as the cube is lifted from wall proximity and reaches a maximum at one-quarter of its side length from the wall [28]. This finding could be applied to side car mirrors, as they are placed away from the vehicle (wall) and the radiated sound peak could be avoided by not placing the mirror a quarter of its side length away.

The Society of Automotive Engineers journal (SAE) is known for its high-quality large-scale work. A comparison of all available simulation methods has been made in terms of wind contribution to interior noise to determine which is the most accurate by validating with an experimental test [15]. The authors' work could provide all the information needed to enter this field of study. Turbulent flow from the side-view mirror creates window vibrations and emits the interior noise in a cuboid cavity [29].

Although Internal Combustion Engine (ICE) vehicles require continuous exterior shape improvement to decrease the drag coefficient and increase efficiency, electric vehicles have several advantages. There are ways to generate energy while travelling, such as brake regeneration and even harvesting energy from the suspension [40–43]. Thus, an electric vehicle could have a higher drag coefficient value but still be more efficient than ICE vehicles.

The vehicle's side mirrors are one of the most significant contributors to wind noise, accounting for around 3–6% of the total drag of the car [44]. A wind tunnel study shows that the vehicle's yaw angle has a strong influence on flow characteristics and aerodynamic noises, with local velocities in this region reaching up to 60% above or 40% below the free-stream velocity, and local turbulence intensities can be as high as 40% [45]. The front side window pressure is slightly affected by the

variation of the mirror's yaw angle with higher frequency [46]. The A-pillar creates highly turbulent airflow; thus, the side view mirror is critical and contributes to wind noise generation [47]. A simulation of a base mirror placed horizontally (0 Degree) or at a 45-degree angle showed no change in terms of aerodynamic forces, but there was an aeroacoustics effect. A 45-degree base is a more desirable position in terms of acoustics generation, as the air is allowed to move more freely around the mirror structure [48,49].

Many factors contribute to side mirror acoustics, such as the shape of the mirror, the position relative to the side window, and others that act as aesthetic merits [50]. A previous article set the optimal mirror wind noise and drag performance. By identifying mirror design constraints. The operating range of these limits determines which geometric shapes provided the best performance in a macro sense. Then the shape is optimized using response surface methods [51]. The pressure on the front side window can reflect the change of the geometry of the side mirror, but it cannot give a coincident correlation to the internal sound pressure [52]. The pressure on the front side window cannot judge the variation of an interior sound field.

The closer the mirror's incline to the mounting plate, the lower the emitted noise in both vertical and lateral directions of the wake. However, an increase in the mirror's aspect ratio increases the induced noise significantly [53]. Adding a bionic shark fin structure could reduce the maximum noise by 7.3 dB, by effectively combing the streamlines and turbulence intensity at the rear of the side mirror to reduce the negative pressure area [54]. The addition of a bionic blade reduce up to 3 dB of emitted noise [55].

Polyhedral mesh requires less simulation time and outputs accurate values and fine mesh to be optimal to use [56]. Based on these researches we will setup our simulations. SIMPLE algorithm is intended for steady flows, while PISO is meant for transient flow [57,58]. It is worth noting that surface roughness has no effect either on aerodynamic forces nor acoustics. The fractional step method is proven to be an efficient time advancement scheme to output acoustic data [59].

While removing mirrors can reduce noise and improve aerodynamics, it is not possible for manufacturing companies to do so due to regulations in the USA. Therefore, modifications to the shape, orientation, and/or position of the mirrors are necessary to achieve the desired noise reduction and aerodynamic improvements. Although many

- Mirror
- Mirror arm (Mirror base)

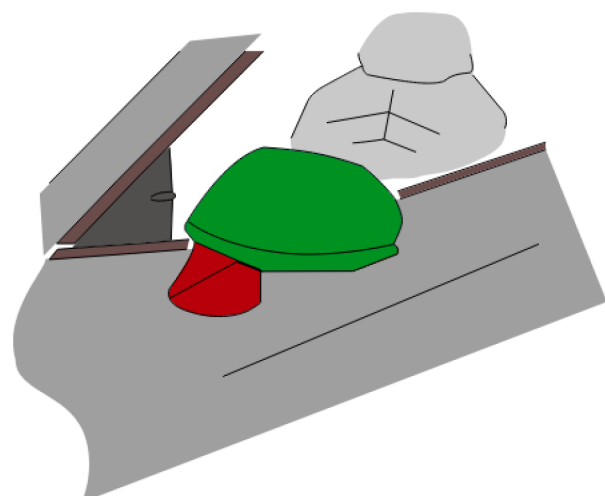


Fig. 2. Isometric view of vehicle showing mirror (Green), and mirror base (Red).

discoveries have been made in previous research about side mirror, the arm connecting the mirror to the vehicle's body is completely ignored (Fig. 2). Fig. 2 illustrates the focus of this journal, as all previous articles focused on the mirror (green region), and completely ignored the base (red region). The effect of changing the mirror base orientation is studied [48], but the optimum angle for the mirror base placement that results least acoustics generation has not been established. The study of every vehicle part is crucial for automotive designers, as every part of the vehicle is designed for optimum position/orientation that results least noise emission or aerodynamic forces. This is the main motivational and objective point of this study. The objective of reducing noise pollution represents a motivational point for this work. This article aims to reduce the noise level generated from the side mirror's base by placing the base at different orientations while the mirror is fixed at constant position.

2. Numerical setup

To conduct the simulation the simulation design must be prepared for in the post processing phase, then when everything is ready and set the processing is initiated, and lastly in the post processing stage the results are extracted.

2.1. Pre-processing

During the pre-processing phase, a design must be created that allows for a fair comparison of all studied cases. The design of the mirror base depends on the design of the rest of the vehicle, particularly the side of the car. A more aerodynamic design requires a vertically straight side cross-section, which rules out an angularly placed mirror or a 90-degree mirror. For example, a high-end luxury sedan has a wide start for the side where the mirrors are located, while the side of the mid-level sedan is almost vertical (Fig. 3). As a result, the mirror for the high-end is angularly placed, and for the mid-level, the mirror is placed horizontally. Therefore, each vehicle side design is compatible with a range of mirror base orientations.

To ensure a fair comparison between angles, the projected area must be the same for each angle studied. Otherwise, the drag coefficient will vary, creating an undesired variable. To fix the base at different angles, the vehicle's side can be designed as a quarter of a circle. This design isolates the mirror's effect and eliminates interference from the A-pillar. The design includes a quarter circle with a radius of 0.2 m and a half circle on the corner of the mirror to guide the base surface, with a radius of 0.05 m. Fig. 4 shows an isometric view of the studied case, with an angle of 90° as an example. Fig. 5 illustrates the dimensions and reference axis for rotation used in this article. Only the mirror and base are modelled and placed on the vehicle's body to represent the actual case. The mirror can be placed and studied in three main positions: on a plate,

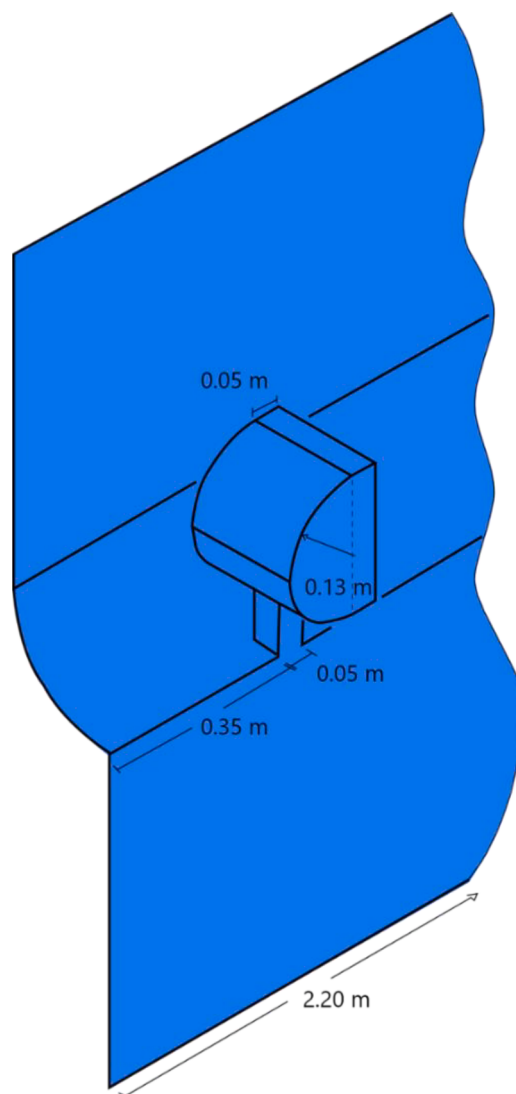


Fig. 4. Isometric view for our case study.

on the side body, or on a vehicle model such as the SAE body [60]. The first two positions produce similar results, but when a vehicle model is included, the A-pillar significantly affects the airflow, resulting in completely different outputs from the other two positions [60].

This research examines 26 cases, each with a different angle value for the mirror base, to obtain the aeroacoustic and aerodynamic force

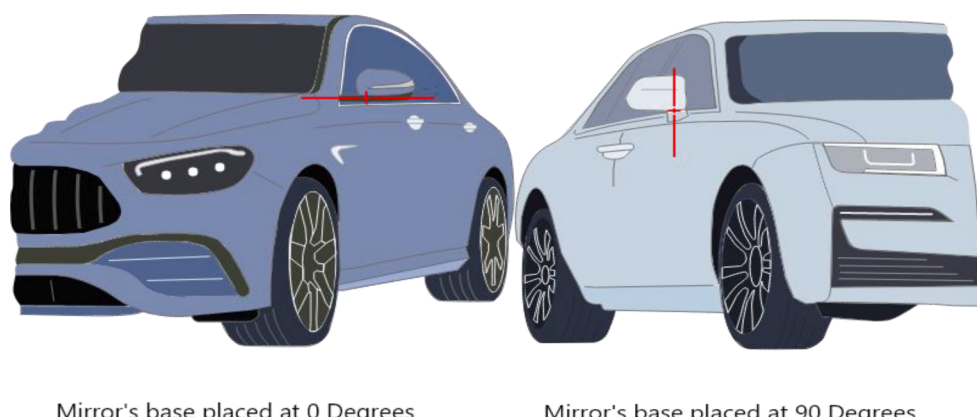


Fig. 3. Side mirrors in two luxury sedans: horizontal in mid-level sedan (left) and vertical in high-end sedan (right).

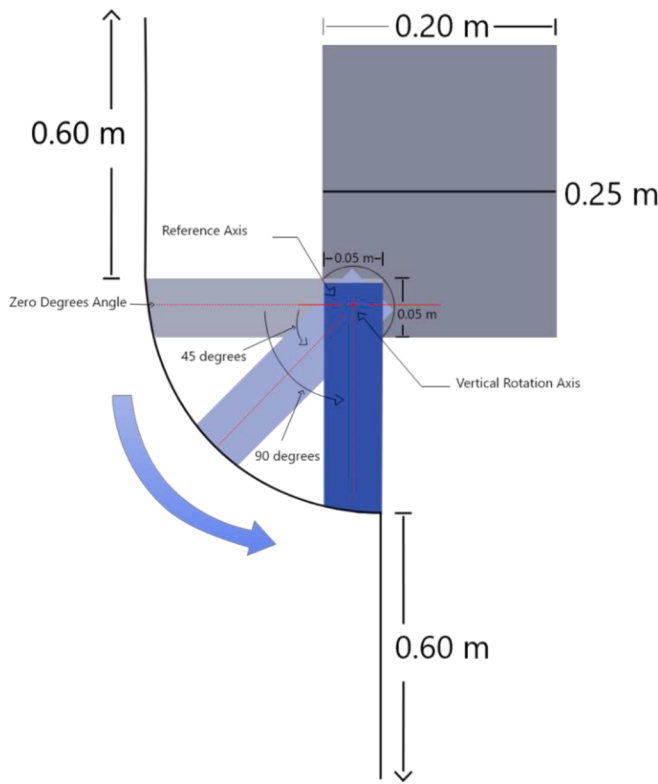


Fig. 5. Front view of the investigated case study.

values. The examined angles range from 0 to 90°, in steps of 11.25 and 1.25°, to cover a wide range. Starting with the 11.25-degree step, the results are analysed, and when there is a significant change in the acoustics or aerodynamic results, a smaller 1.25-degree step is used to obtain more precise data. The 1.25° step is chosen for angles ranging from 50 to 61.25, and 80 to 90°, where the results showed significant variation.

2.2. Processing

In the processing phase, this article utilized the available resources to simulate the result, with the most attainable efficiency. As other research had high end CPUs with CPU run time lasting for days, this can't be done in our case, due to the sheer scale of work required, and availability of funding. So, the research considered the efficiency as an important factor in the decision of the method used. For example, using polyhedral mesh as it is more efficient and outputs accurate results, although it has less cells than tetrahedral mesh [56].

Based on the literature review made and learning from previous experiences of trial and error to find the settings that provide perfect or the most accurate results this work utilizes the Scale Adaptive Simulation viscous model, as SAS shows accurate results simulating acoustics [61]. As mentioned in the introduction, the two main components creating noise are the convective and acoustic components. It is worth noting that acoustic waves are dependent on compression and decompression of air molecules to create waves which are sound. However, in our incompressible case, the fluid loses this component and doesn't generate the acoustic component but just the convective. This is not a problem, because of the small amplitude of the acoustic component.

The current turbulence models suffer from the lack of an underlying exact transport equation [62]. This lack of an exact solution for the omega and epsilon equations leads to not accurately solution for large scales. The SST-SAS transport equations in ANSYS are defined as:

$$\frac{\partial p_k}{\partial t} + \frac{\partial}{\partial x_i} (\rho u_i k) = G_k - \rho c_\mu k \omega + \frac{\partial}{\partial x_j} \left[\left(\mu + \frac{\mu_t}{\sigma_k} \right) \frac{\partial k}{\partial x_j} \right] \quad (1)$$

$$\begin{aligned} \frac{\partial \omega}{\partial t} + \frac{\partial}{\partial x_i} (\rho u_i \omega) &= \alpha \frac{\omega}{k} G_k - \rho \beta \omega^2 + Q_{SAS} + \frac{\partial}{\partial x_i} \left[\left(\mu + \frac{\mu_t}{\sigma_\omega} \right) \frac{\partial \omega}{\partial x_i} \right] \\ &+ (1 - F_1) \frac{2\rho}{\sigma_{\omega,2}} \frac{1}{\omega} \frac{\partial k}{\partial x_j} \frac{\partial \omega}{\partial x_j} \end{aligned} \quad (2)$$

Where p is the pressure, t is the time, i, j , and k are unit vectors in ∂x variants, F is the force, ρ is the density, and the value is found by trial and error to be the optimum value to output accurate results, also α, β, ω , and σ are all constants with values determined in literature. Q_{SAS} is formulation results in an additional term in the ω -equation of the SST model added to the right hand side of the SST ω -equation and is shown in Eq. 31 in Egorov and Menter's work [63]. A more detailed derivation for the equations is done by Egorov and Menter [63,62].

The process by which sound reaches the driver involves several steps: first, the air causes fluctuating pressure on the side glass, then the glass transmits the waves inside the medium, and finally, the vibrations created in the inner air cabin reach the driver's ears. To simulate this process, researchers use a model known as Aero-Vibro-Acoustics, which requires a three-part process involving ANSYS fluent, ANSYS mechanical structure, and ANSYS harmonic acoustics. This process measures the turbulence created by the vehicle outside, simulates the solid transmission with ANSYS mechanical, and then uses ANSYS harmonic acoustics to create noise inside the cabin as a vibrator.

In this study, we focused on the outside window to compare alternative angle positions for the same scenario. It is worth noting that many applications are interested in the sound radiation from a uniform flow over a stationary object. For example, in model testing conducted in wind tunnels, a uniform steady flow is used at large distances from the region of turbulence that causes the sound. Although this study did not use the procedures explained in the previous paragraph, it is still able to accurately extract acoustic data using the Ffowcs-Williams & Hawkins (FFW) formulation in Fourier series format with Hanning window. The mirror and base were set as the source, and 13 receivers were placed on the vehicle side to collect data (Fig. 6). Ffowcs-Williams and Hawkins have been verified to output precise and accurate results [64].

The Ffowcs-Williams and Hawking model (FW-H) is an inhomogeneous wave equation that is derived from the continuity and the Navier-Stokes equations. The FW-H equation is written as follows [65]:

$$\begin{aligned} \frac{1}{a_o^2} \frac{\partial^2 p'}{\partial t^2} - \nabla^2 p' &= \frac{\partial^2}{\partial x_i \partial x_j} \{ T_{ij} H(f) \} - \frac{\partial}{\partial x_i} \{ [P_{ij} n_j + \rho u_i (u_n - v_n)] \delta(f) \} \\ &+ \frac{\partial}{\partial t} \{ [P_o v_n + \rho (u_n - v_n)] \delta(f) \} \end{aligned} \quad (3)$$

Where, u_i is the fluid velocity component in the x_i direction ($i = 1, 2, 3$), u_n is the fluid velocity component normal to the surface $f = 0$, v_i and v_n are the surface velocity component in the x_i direction, and normal to the surface, respectively, $\delta(f)$ is the Dirac delta function, and $H(f)$ is the Heaviside step function. If an equation of the form $f = 0$ defines the surface S , and is such that $f < 0$ in region 1 and $f > 0$ in region 2, then a surface integral over S can be replaced by a volume integral over V with the integrand [66].

To obtain the solution for a free-space flow, the wave equation is integrated analytically, assuming that there are no obstacles between the sound sources and the receivers. The resulting solution involves a combination of surface and volume integrals. In the case of low subsonic flow, the contribution of the volume integrals is considered negligible. As a result, the solution obtained using ANSYS Fluent is:

$$p'(\vec{x}, t) = p'_T(\vec{x}, t) + p'_L(\vec{x}, t) \quad (4)$$

Where,

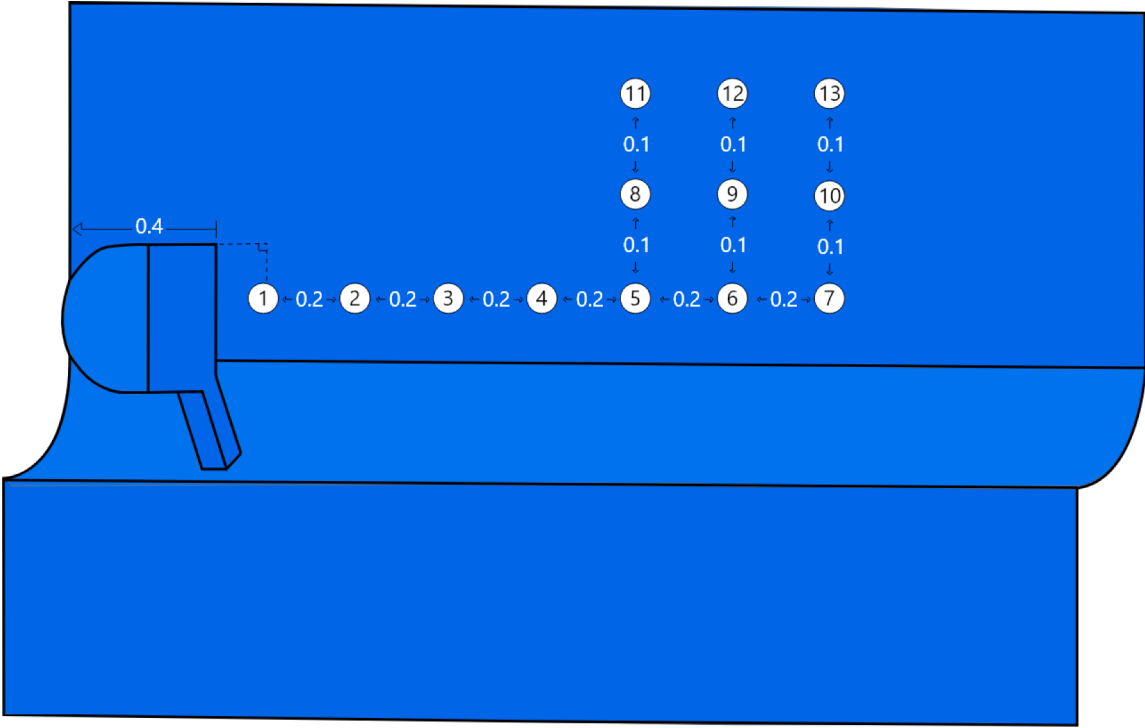


Fig. 6. Receivers location on the vehicle's side.

$$4\pi p'_T(\vec{x}, t) = \int_{f=0} \left[\frac{p_o(\dot{U}_n + U_n)}{r(1 - M_r)^2} \right] dS + \int_{f=0} \left[\frac{p_o U_n \{ r\dot{M}_r + a_o(M_r - M^2) \}}{r^2 (1 - M_r)^3} \right] dS \quad (5)$$

$$\begin{aligned} 4\pi p'_T(\vec{x}, t) = & \frac{1}{a_o} \int_{f=0} \left[\frac{\dot{L}_r}{r(1 - M_r)^2} \right] dS + \int_{f=0} \left[\frac{L_r - L_M}{r^2 (1 - M_r)^2} \right] dS \\ & + \frac{1}{a_o} \int_{f=0} \left[\frac{L_r \{ r\dot{M}_r + a_o(M_r - M^2) \}}{r^2 (1 - M_r)^3} \right] dS \end{aligned} \quad (6)$$

Where,

$$U_i = v_i + \frac{\rho}{\rho_o} (u_i - v_i) \quad (7)$$

$$L_i = P_{ij} \hat{n}_j + \rho u_i (u_n - v_n) \quad (8)$$

Eq. (7) is a form of the continuity equation, which relates the flow velocity of a fluid to its density and mass flux. The form relates the velocity of a fluid (U_i) to the velocity of a reference frame (v_i), the density of the fluid (ρ), the density of the reference frame (ρ_o), and the mass flux ($u_i - v_i$) between the fluid and reference frame. **Eq. (8)** is a representation of the lift force acting on a body. (L_i) is the lift force in the i direction, P_{ij} is the pressure tensor in the i,j direction, \hat{n}_j is the unit normal vector in the j direction.

To accurately capture the acoustics values of the turbulent airflow after interacting with the side mirror, a transient model that changes with respect to time is desired. However, for aerodynamic forces, a steady-time solution can output values when the simulation reaches a steady state. In this manuscript, both transient and steady-state models are used to output the desired acoustics values and aerodynamic forces, respectively.

Given the airflow speed of 40 m/s and the occurrence of vortices, the simulation is run until 0.0825 s. The mesh refining process is crucial to obtain accurate results, as it represents the size of the studied part, where the pressure and velocity components are calculated at the inlet

and outlet for each element. In this work, ANSYS automatic mesh generator is first applied, then the mesh base size is constantly reduced in a trial-and-error method until a constant output is achieved. The desired value of the residual is set by the user, and the solver keeps solving until the number of iterations set or the residual value is reached.

Choosing a very small element size can result in more precise results, but it can also lead to long computational time and require high-end CPUs. Conversely, a large element size will yield inaccurate results. For the mesh refining process, ANSYS Fluent generates an automatic mesh at first, and the solver runs, and the results are recorded. Then a mesh sizing method is applied, taking the mirror and side body surfaces and applying 50 mm element size, then constantly decreasing the value to 10 mm with a step size of 5 mm. At each step of the mesh refining process, the solver is run, and data is recorded. **Fig. 7** shows results are in 7 N range, so results are accurate at smaller mesh size of 300×10^3 elements and above. Simulating for the drag force is sufficient as the values are connected with acoustics.

In the setup phase the mesh is switched to polyhedral thus changing the mesh size as shown in **Table 1**. **Table 2** shows the methodology used in ANSYS fluent setup. The mesh used is divided into 9 zones with total of 351,555 nodes. **Fig. 8** shows the mesh used in the case study, which includes edges, faces, and partitions. As previously mentioned in the introduction, a polyhedral mesh element was chosen as it is considered the optimal meshing method for CFD analysis. **Fig. 8** shows the coloured boundary conditions with labels, where there are two views, one without the outside boundary wall, and other with the boundary wall. In **Fig. 8** the purple surface is the inlet and the red surface is the outlet, the grey part is the mirror and car surface, and the green wall is the boundary wall labelling the study area. The wall roughness is not important and its effect is still unclear [67], the DrivAer wall is set as default.

In CFD simulation the geometry is designed first (**Fig. 2**) then an enclosure is created that surround the body and act as the boundary of the studied area, the boundary conditions are shown in **Table 3** with reference to **Fig. 8** colors.

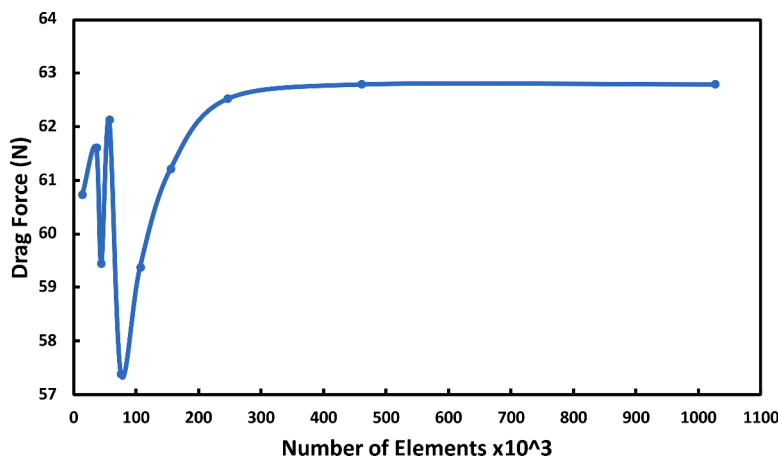


Fig. 7. Mesh refining for studying the optimum mirror base orientation that results lowest aeroacoustics and/or aerodynamic forces, the drag force (N) is plotted with respect to the number of elements.

Table 1
Polyhedral mesh analysis and size.

Polyhedral	Automatic	Modified
Cells	4401	64,768
Faces	25,093	421,606
Nodes	19,289	351,555
Partitions	32	32

Table 2
The methodology used in ANSYS fluent.

Title	Setup
Flow	Incompressible
Turbulence model	Scale Adaptive Simulation
Air Flow Velocity	40 m/s
Reynolds Number	5.95×10^6
Algorithm	PISO
Gradient	Least squares based
Warped Face Gradient Correction	Applied
Mesh	Polyhedral
Acoustics	FFW
Type	Pressure Based

2.3. Post processing

The ANSYS solver outputs pressure fluctuations that are recorded at each receiver location, but the results can be difficult to interpret. To better represent the data, a Fourier Transform with a Hanning Window is used, with Sound Pressure Level in decibels plotted on the Y-axis and Frequency on the X-axis. The data is extensive, so we established several factors to determine the best base angle. For instance, since the Fourier transform is more affected by magnitude at lower frequencies than at higher frequencies, this will be taken into account. Additionally, the receivers from 5 to 13 in Fig. 9 are prioritized as they are closer to the drivers' ears.

3. Results and analysis

The result obtained for the transient simulation are the aeroacoustics values, and steady state simulation results the aerodynamic forces values. The results are outputted from ANSYS solver and presented in order to conclude a specific value for the side mirror base orientation that results the least acoustics generation and/or aerodynamic forces.

3.1. Aeroacoustics analysis

The data obtained is very hectic in values because Fourier transform is applied, and the results show continuous up and down movement in values. Therefore, several procedures were used to determine the best base angle position out of the 26 cases studied. For example, since Fourier Transform results in frequency related parameters, and in terms of sound the magnitude of the SPL at lower frequency is more important than at the higher frequency noise levels, as they are more audible to the driver. However, in this work the range of frequencies is 1 – 1000 Hz which is all audible to humans and is considered noise. Furthermore, the 13 receiver's location should also be considered, as the receivers from 5 to 13 in Fig. 9 are more important since they are closer to the drivers' ears. The generated noise closer to the occupant's ears are more important than noise away from the ears. Fig. 9 is designed with dimensions taken based on Toyota Camry 2016 model to figure out where the driver's location will be while travelling inside the vehicle.

The result consists of many up and down curves since it is a Fourier Series (Fig. 10), so in order to better understand the data and be able to output a result, a 4th order polynomial is obtained for each line, to better see the results (Fig. 11). The order of polynomial is chosen as the most accurate representation by taking the values at the start of the curve. For example, at 78.75° in receiver 10 the original results start at 77.4 dB, and when applying polynomial, the starting value is as follows; 2nd order 71, 3rd order 74, 4th order 76, 5th order 80, and 6th order is 82 dB. This shows that the 4th order is the most accurate representation since the value obtained is closest to the original starting value (error 1.8%). The data starts from 10 Hz to 910 Hz, but the first 100 Hz is removed because of undeveloped flow separation regions, as well as the last 10 Hz [68].

The obtained results show SPL reaching almost 100 dB (Fig. 10) and this might seem to the reader as a huge value, but it is not. Although SPL is measured in dB it is different from the sound amplitude which is also measured in decibels. However, if the sound amplitude reaches above 85 dB could result in permanent ear injury for humans. The SPL is found from sound pressure as follows:

$$SPL(dB) = 10\log_{10} \left(\frac{p^2}{p_o^2} \right) \quad (9)$$

Where, SPL (dB) is the sound pressure level in dB, p is the sound pressure in Pa, and p_o is the reference sound pressure level which has a fixed value of $20 \mu Pa$.

The data shows that receiver 1 (Fig. 10) recorded the highest SPL value (close to a 100 dB), since closest to the mirror, then the maximum SPL value kept decreasing as in receiver 13 till it reached around 70 dB. The resulted data obtained had accumulated error, and some values at

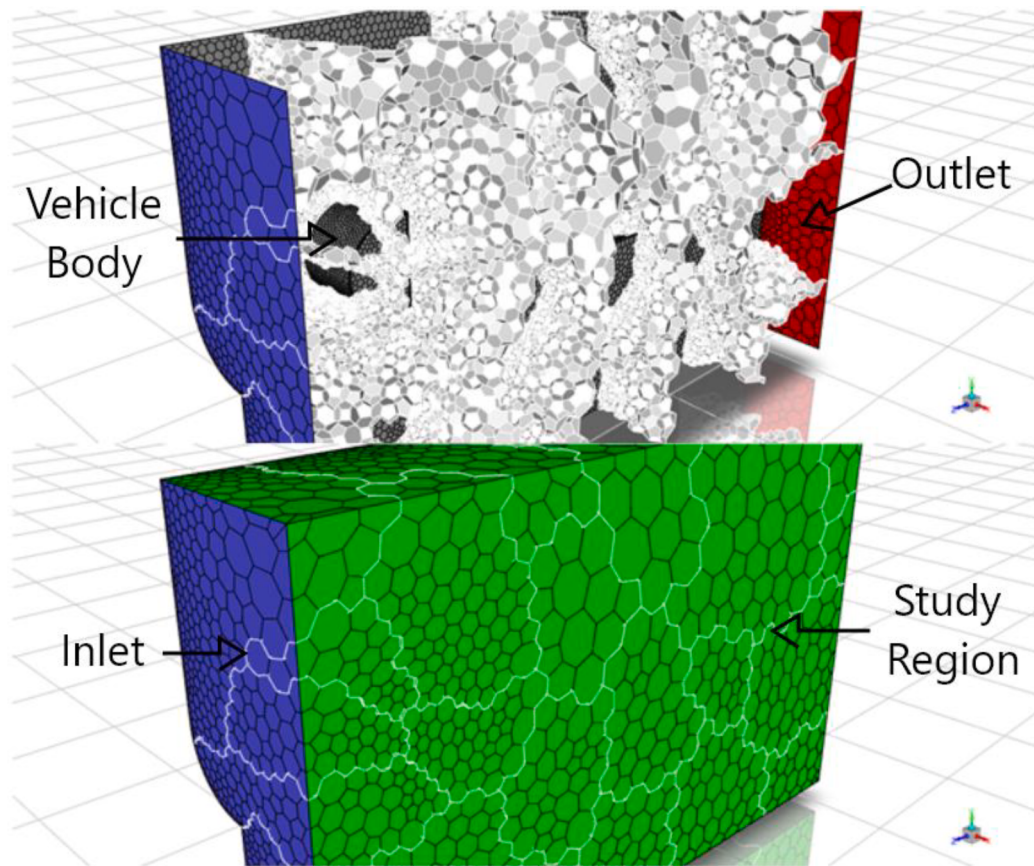


Fig. 8. Mesh display for the investigated case, view of the case study, without the outside boundary wall (top), and with the boundary wall (bottom).

Table 3
Boundary conditions with reference to Fig. 8.

Boundary	Setup
Inlet (Purple)	40 m/s velocity inlet
Outlet (Red)	Pressure outlet atmospheric
Mirror and Base (Light Grey)	No-slip wall surface
Vehicle body (Light Grey)	No-slip wall surface
Top and bottom wall (Green)	Slip, zero shear wall
Wall opposite to vehicle body (Green)	Slip, zero shear wall

higher frequencies reached a negative value and this is physically impossible. All these negative errors were disregarded.

To choose the optimal angle we are concerned with the lowest SPL value over the longest period in frequency. Each receiver is studied based on lowest SPL and the duration it remains the lowest, and the values are written in table format and shown in Table 4 for every receiver. As an example, receiver 1 SPL vs frequency with different mirror base angle positions in Fig. 11 is taken and the lowest value is labelled for the frequency range it remains the lowest (Fig. 12).

Table 4 summarize the results obtained by each receiver where the lowest curve value representing the mirror base angle is mentioned and the duration it remains the lowest. From the observed data, few receivers have different base angle that results lowest generated acoustics for the longest frequency range, and the results are shown in Table 5.

After examining a variety of mirror base angles (Table 5), it is concluded that a mirror base positioned at an angle of 85° from the horizontal level gives the lowest SPL (dB) for the longest frequency range as indicated in all receivers, with values plus and minus 3.75 around the 85 values. This could be related to more air flow passes in between side and mirror, and it redirects turbulent flow from the mirror away from the side window. To illustrate, the more the mirror base angle

value the further it is from the side body, thus allowing more linear airflow to pass unaffected by the geometry at the aide body.

The Turbulent Kinetic Energy (TKE) is associated with eddies formed in turbulent flow, it is characterized by the Root Mean Squared (RMS) velocity fluctuations as shown in Eq. (10), in (m^2/s^2) . The velocity components are solved numerically from the turbulent intensity that is taken as 0.5% in this work. The TKE is an important parameter in understanding acoustic generation, as the bigger the TKE value the higher the velocity fluctuations. Velocity fluctuations create vortices which as mentioned before generate acoustics. Therefore, the less the TKE, the lower the acoustic emission. A visual comparison is made between the concluded optimum range of angles ($85 \pm 3.75^\circ$) and another angle with high SPL output to prove the obtained results (45°). Fig. 13a and b show a comparison between 85 and 45 base mirror angles in the range of $10 m^2/s^2$ TKE. Fig. 13a shows TKE value in isosurface isometric view, and Fig. 13b shows TKE in isosurface side profile view.

$$TKE = \frac{1}{2} ((\overline{u'})^2 + (\overline{v'})^2 + (\overline{w'})^2) \quad (10)$$

where, u' , v' , and w' are the velocity components in the x, y, and z axis.

Fig. 13b gives a side profile view which shows the concentration of the eddies and vortices, and at the 85° the shape spreads out to the lower part of the vehicle, while at 45° it focuses on the driver's window, causing high noise emission close to the driver's ears. These results prove the validity of the outcomes of this study as there is large difference in SPL when changing the mirror base position.

In terms of frequency the Strouhal number is usually used to determine the predominant frequency value f_s in the following equation:

$$Sr = \frac{f_s L}{U_\infty} \quad (12)$$

Where L is the characteristic length, and U_∞ is the freestream

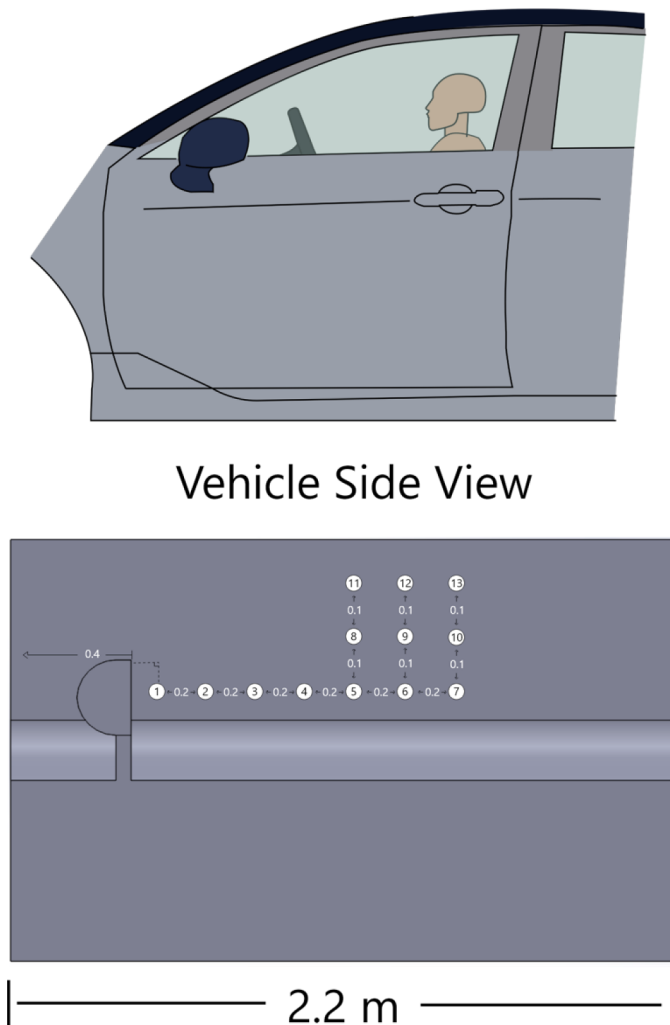


Fig. 9. Driver side in vehicle modelled and receivers' location are placed near the occupants' ears.

velocity. The Strouhal Number (Sr) is found to be a function of Reynolds number. However, in this work the Reynolds number equal to 5.95×10^6 which is turbulent flow and results vortex shedding over a wide range of frequencies, which cannot be determined analytically.

Noise at 300 Hz is considered harmful and could cause headaches when subjected to for long periods of time, and the results obtained for each mirror arm orientation show the spread of values around 300 Hz

[69]. To measure the difference of SPL at different receivers, the frequency value is fixed at 300 Hz and the 85-degree base is compared with 45° as shown in Fig. 14. Since the range of $85 \pm 3.75^\circ$ are chosen to be the optimum position to result in the lowest noise emission possible. To prove the difference in results between angles a comparison is made between the optimum 85° and 45° . The results show that there is a 40-degree difference, but the noise emitted difference is significant with a value up to 32 dB in SPL (Fig. 14).

In Fig. 14 the value of SPL at receivers 1 and 2 seem close between the two angles, but as the receivers move away from the mirror the difference appears more and more significant, reaching around 32 dB at receiver 11. A difference of 32 dB is huge in aeroacoustics optimization, as previous work could result in ~ 7 dB modification [54]. This observation is logical since the area close to the mirror mainly shows the mirror effect as it is the larger geometry but as the distance increases the effect of the base mirror starts to show. Again, this proves our decision is correct and our objective is valid and influences vehicle comfort and ride quality, by reducing the emitted noise.

3.2. Aerodynamic forces analysis

Results for aerodynamic forces (Fig. 15) are obtained in a separate simulation using a steady state that uses K-Omega model unlike the acoustics model which is simulated in transient flow. The figure is combined with the SPL acoustic values taken at receiver 13 since it is the closest to the driver's ear at a fixed frequency of around 300 Hz. The 300 Hz value is chosen because the values there are spread out and easily differentiable as can be seen from the acoustics plot (Fig. 15). In terms of aerodynamic forces, the drag side and mirror are almost constant for every angle, and this is because the surface area is constant, and as [70] concluded by the drag equation, that drag is directly proportional to the projected area.

The efficiency and precision of the developed comparison model is proven by the obtained aerodynamic drag force. The constant projected area was maintained to isolate the acoustics effect, and the constant drag force serves as an indicative parameter for the validity of the model. In contrast, the lift force varies constantly due to the mirror acting as an aircraft wing, lifting the vehicle upwards, as discussed by [71]. The results consider the positive y-axis pointing upward, so the higher the value of the lift force, the worse it is for vehicle stability. Unlike aircraft, where upward lift is desirable for flying and taking off, vehicles require downward lift for stability, as the more the vehicle hugs the ground, the better.

Although changing the angle of the base mirror increases the lift force, the change is relatively small, with a maximum value of around 15 N. This value is incapable of lifting the vehicle or causing significant stability changes, as most vehicles weigh more than 1000 Kg. The slight

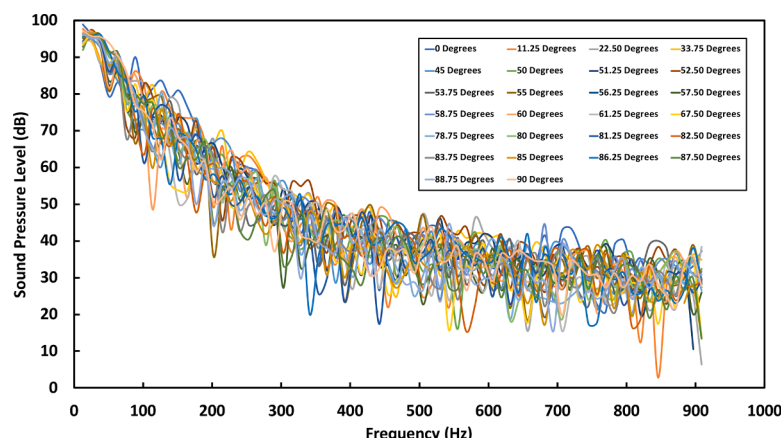


Fig. 10. Receiver 1 at different mirror base angles original results from ANSYS solver.

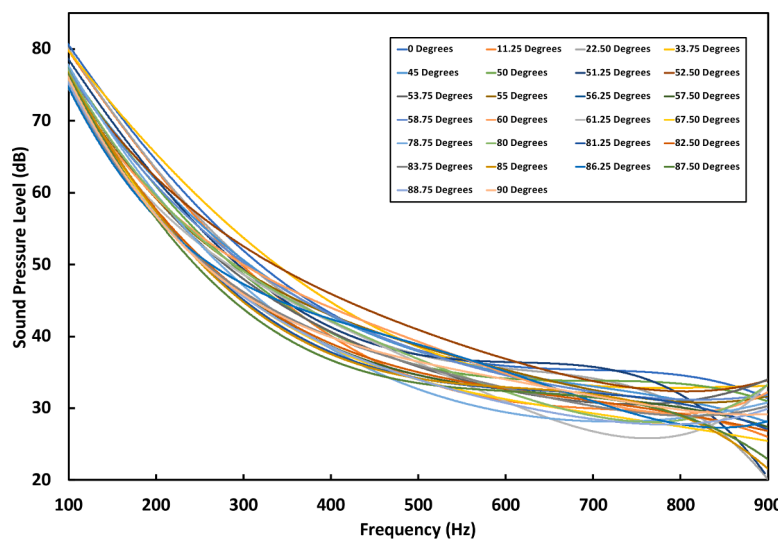


Fig. 11. Receiver 1 at different mirror base angles with 4th order polynomial.

Table 4

Receiver 1 – 13 values for the SPL magnitude for the base angle position and the duration it maintains being the lowest in frequency (Hz).

Receiver 1 Angle in degrees	Frequency duration (Hz)	Receiver 3 Angle in degrees	Frequency duration (Hz)	Receiver 5 Angle in degrees	Frequency duration (Hz)
86.25	100	86.25	90	88.75	20
87.5	260	85	210	85	390
78.75	190	87.5	130	78.75	140
61.25	170	78.75	60	53.75	100
67.5	10	83.75	200	55	30
85	40	50	50	51.25	120
51.25	30	22.5	60		
Receiver 2 Angle in degrees	Frequency Duration (Hz)	Receiver 4 Angle in degrees	Frequency Duration (Hz)	Receiver 6 Angle in degrees	Frequency Duration (Hz)
86.25	100	85	360	88.75	90
88.75	200	78.75	150	85	280
87.5	190	83.75	210	90	50
11.25	40	87.5	20	78.75	50
61.25	160	22.5	60	67.5	80
11.25	35			55	160
50	75			87.5	90
Receiver 7 Angle in degrees	Frequency Duration (Hz)	Receiver 9 Angle in degrees	Frequency Duration (Hz)	Receiver 11 Angle in degrees	Frequency Duration (Hz)
88.75	90	87.5	80	85	380
85	220	85	200	83.75	180
90	130	83.75	220	57.5	110
67.5	60	55	200	50	130
55	210	51.25	100		
87.5	90				
Receiver 8 Angle in degrees	Frequency Duration (Hz)	Receiver 10 Angle in degrees	Frequency Duration (Hz)	Receiver 12 Angle in degrees	Frequency Duration (Hz)
85	410	87.5	95	87.5	30
78.75	130	85	195	85	260
55	90	90	120	90	100
50	70	78.75	90	78.75	100
51.25	40	50	90	83.75	100
22.5	60	55	110	50	210
		83.75	100		
Receiver 13 Angle in degrees	Frequency Duration (Hz)				
87.5	120				
85	200				
83.75	190				
55	140				
50	60				
22.5	90				

lift force is due to the air passing upwards faster than downwards over the body, creating a pressure difference, where the lower side has more pressure and goes upwards to the lower pressure area [72]. At a 0-degree

angle, the lift force is at its minimum, which is related to the turbulent air created from the side of the vehicle under the mirror. The lift force value keeps increasing and then decreases sharply for the 90-degree

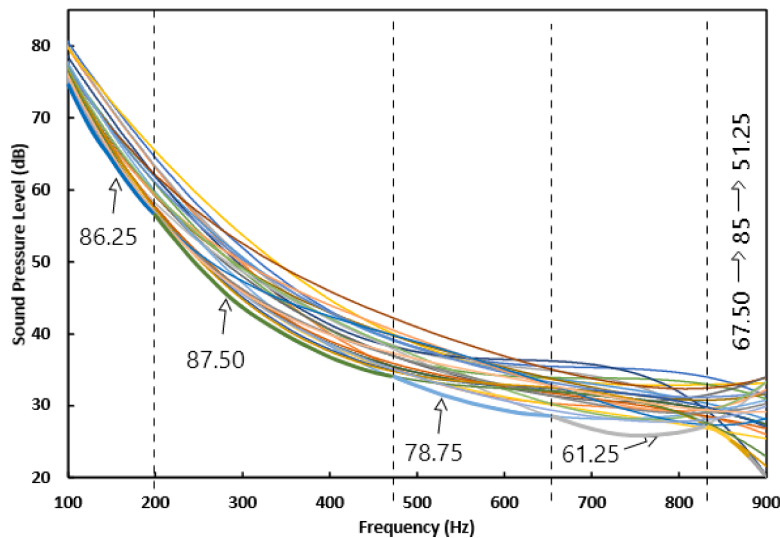


Fig. 12. Receiver 1 SPL vs frequency with different mirror base angle positions, with the lowest angle position and the range of frequencies it remains the lowest.

Table 5

Each receiver number and the mirror base angle that results lowest generated SPL for the longest frequency period.

Receiver number	Mirror base angle (Degrees)
1	87.50
2	88.75
3	85
4	85
5	85
6	85
7	85
8	85
9	83.75
10	85
11	85
12	85
13	85

angle. This effect is due to the separation and wake region created by the mirror and base being very close, resulting in a large zone of low-pressure wake. Adding the Sound Pressure Level (SPL) to Fig. 15 provides more insight into the results and confirms that the angle of 85° and the surrounding 3.75° have the lowest noise emission.

Fig. 15 shows the obtained aerodynamic forces for the mirror part (mirror and mirror base) plotted with respect to the mirror base angle. In addition, the SPL at 300 Hz for receiver 13 is added to the plot with its y-axis (right). The case of the mirror arm placed at 85° is also run with Large Eddy Simulation (LES), which is a highly accurate, precise, and computationally demanding turbulence model. However, the results obtained are similar to the SAS model results, confirming the validity of the results shown here.

3.3. Results validation

Since this article explores a research gap that has not been studied before, experimental validation is not available in the literature yet. However, the obtained results follow an expected trend of past articles that studied the mirror such as the work done by Belamri et al. [73], and this is used to validate the results. The experimental data done focused on the side mirror part with similar dimensions and resulted up to 1000 Hz noise and with similar starting SPL value of around 100 dB, which is similar to the obtained results in this article [73]. Therefore, the obtained results are validated, as they show similar trend in values and behaviour of results. Fig. 16 shows a comparison between the results

obtained and the already existing numerical and experimental results [56,73]. The result shows good correlation with the trend of results. The different values are due to the fact that the experimental results have considered only the mirror, but in this article the mirror base is considered as well, so results should not have similar values.

In experimental results, the lowest noise possible is the ambient noise, which is around 60 dB, unlike in simulation where results could reach really low SPL values. The existence of a minimum noise explains the difference in results between simulation and experimental. When comparing the obtained results with existing, a similar trend in behaviour and range of frequencies is observed. However, there is also a slight shift in values due to slightly closer receiver position towards the mirror, and as mentioned previously, that the closer the receiver to the mirror the higher the maximum SPL value. To illustrate, the current obtained results is at 0.1 m from the mirror part [73], and in this manuscript, receiver 1 is 0.2 m away from the mirror. Receiver 1 is also not in the wake region of the mirror, but it is placed on the vehicle's side, unlike experimental setups where the receiver is in the wake of the mirror [73]. The difference in the setup explains the difference in results, but the results behave in similar manner when increasing the frequency values.

4. Conclusion

The results of this study demonstrate the effectiveness of the simulation model that was utilized, specifically the combination of the SAS viscous model and the FW-H acoustic model, which yielded highly accurate results. While many researchers tend to rely on computationally intensive models such as LES or DES in conjunction with the FW-H acoustic model, the findings of this study provide evidence that the SAS and FW-H models are sufficient in outputting accurate and precise results.

The outcome of this research is revolutionary for the automotive industry, as a simple change of angle from 45 to 85° results in a significant difference in noise emission is noticed, reaching up to 32 dB. The difference recorded is mind-blowing compared to the minor design change. This research benefits the automotive industry as the designers can decrease cabin noise by following the output of this article, this will result in an improvement in vehicle ride quality, since the mirrors are responsible for large portion of noise for the driver, this trivial design change can make any automotive company reach luxury level of comfort without the addition of extra weight of noise dampening material.

This research has significant implications for the automotive industry especially for electric vehicles, which are gaining popularity in the market due to their quieter operation compared to traditional

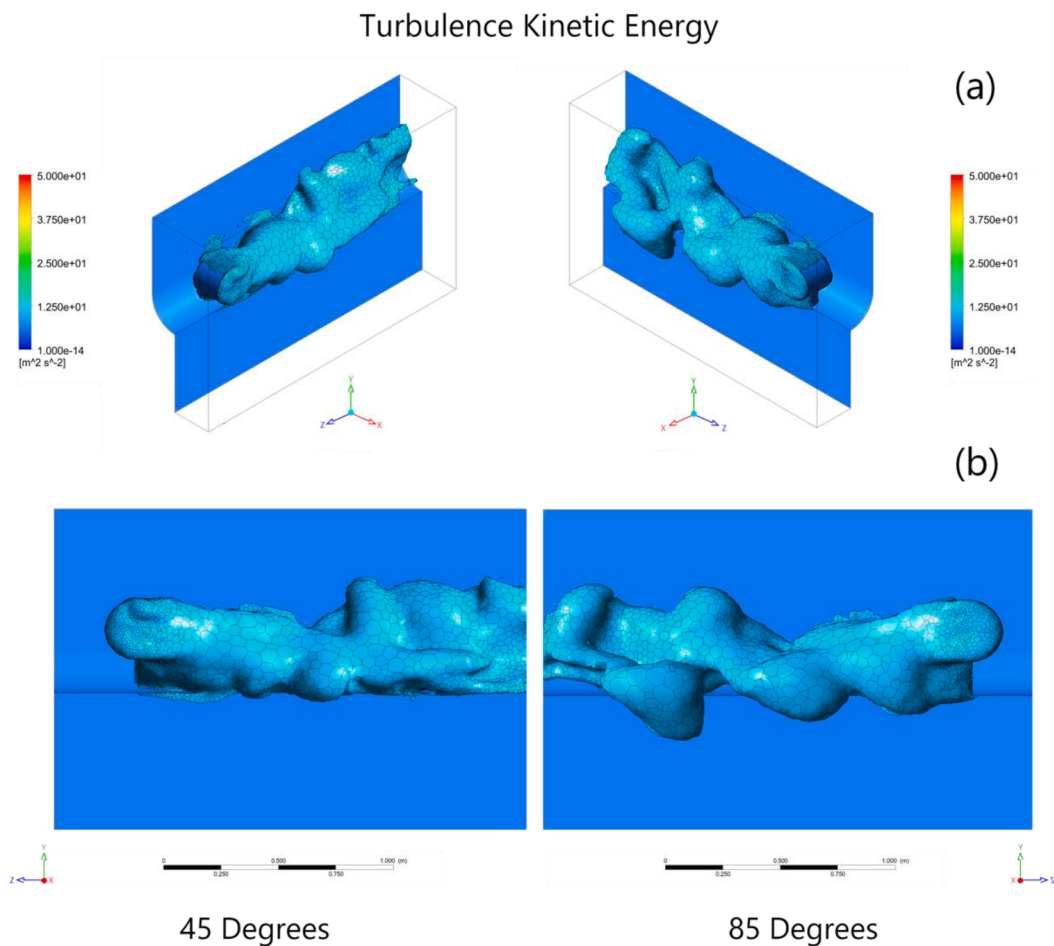


Fig. 13. Turbulence kinetic energy isometric view (a) and side profile view (b) comparison between 45 and 85°.

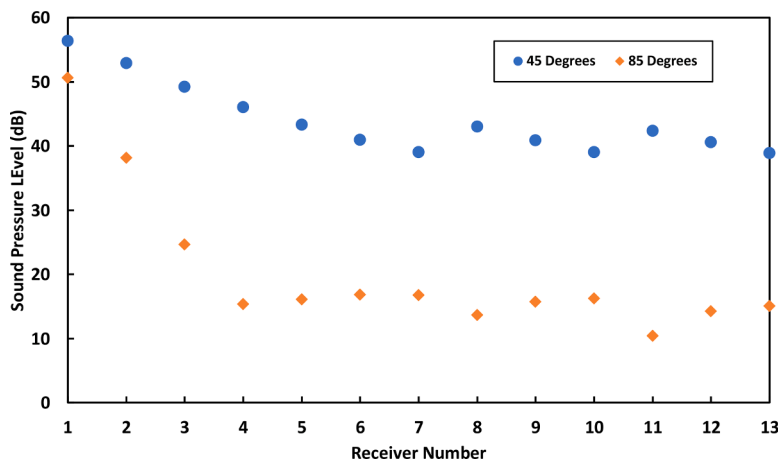


Fig. 14. SPL at different receivers for fixed frequency of around 300 Hz comparison between 45 and 85°.

internal combustion engine (ICE) vehicles. However, wind noise can be more noticeable in electric vehicles due to the absence of an engine.

It is concluded that the optimal mirror's base angle relative to the vertical axis at the mirror and base connection in aeroacoustics is 85 $\pm 3.75^\circ$ angle in terms of aeroacoustics, and relatively the aerodynamic forces. As results show the if the base of the mirror is placed at 85 $\pm 3.75^\circ$ from the horizontal axis this results in least noise emission compared to all other angles studied. Furthermore, the aerodynamic force analysis shows almost constant drag force, but changing lift force, as increasing

the angle increases the lift force until reaching 90° where the force drops significantly but still isn't as small as 0°. Although there is a change in lift force the maximum change is around 15 N, and this small increase doesn't affect the vehicle stability as much as the effect on reducing noise emission.

Declaration of Competing Interest

The authors declare that they have no known competing financial

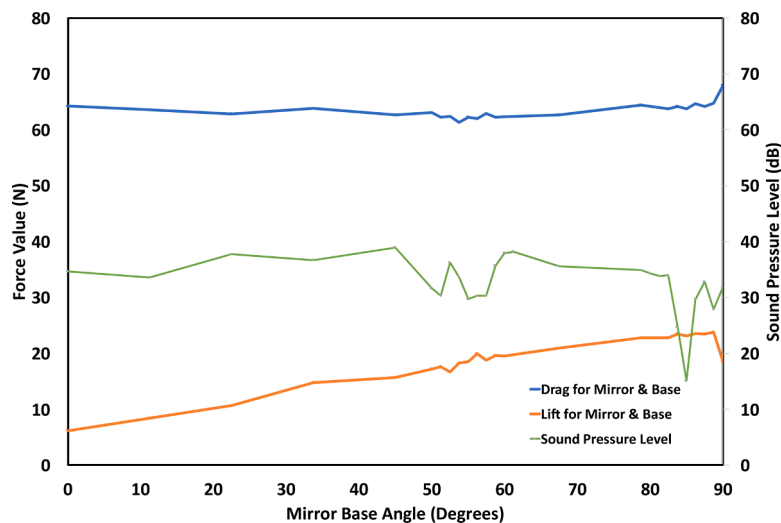


Fig. 15. Aerodynamic forces of drag and lift and the SPL in dB at receiver 13 with fixed 300 Hz plotted at different side mirror orientations.

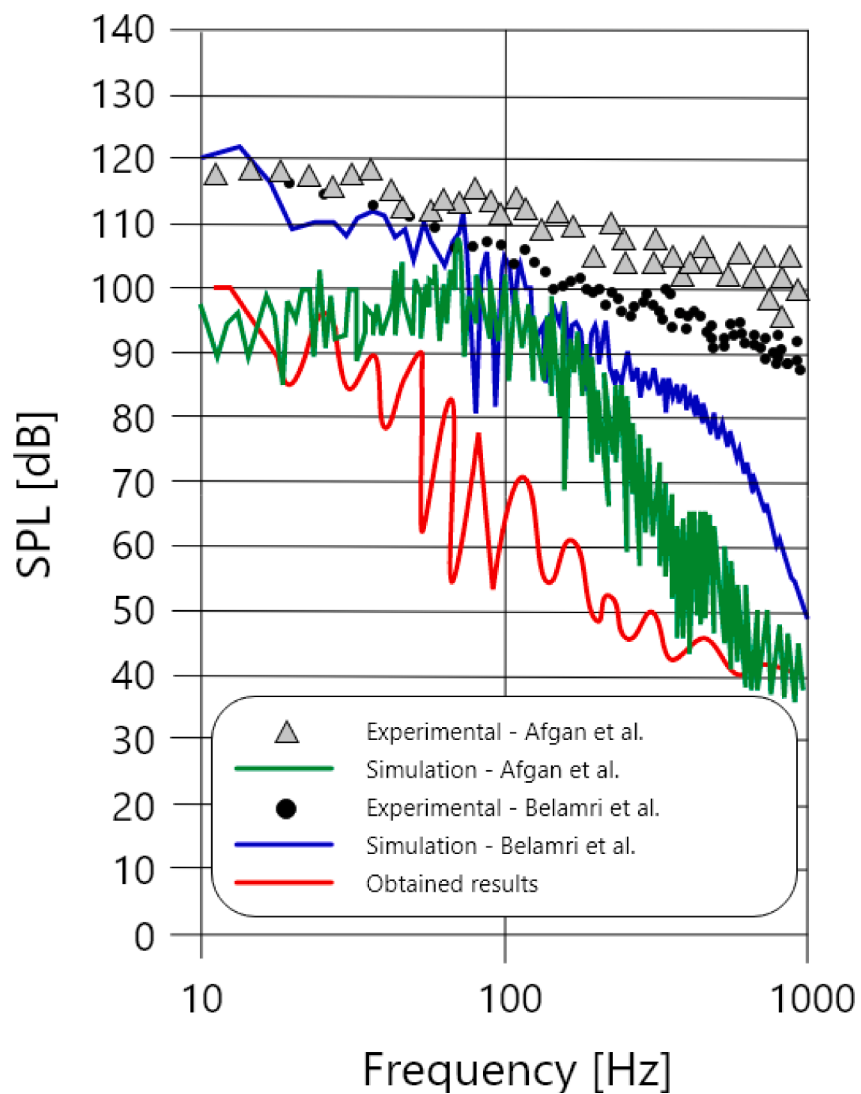


Fig. 16. Obtained results compared with existing results in literature.

interests or personal relationships that could have appeared to influence the work reported in this paper.

Data availability

Data will be made available on request.

Acknowledgements

The authors would like to acknowledge UAE University for providing the facilities and funds through Materials library (#31N392) - Industry 4.0 district project.

References

- [1] S.A. Stansfeld, M.P. Matheson, Noise pollution: non-auditory effects on health, *Br. Med. Bull.* 68 (2003) 243–257, <https://doi.org/10.1093/bmb/ldg033>.
- [2] L. Goines, L. Hagler, Noise pollution: a modern plague, *South Med. J.* 100 (3) (2007) 287–294.
- [3] N. Maisonneuve, M. Stevens, M.E. Niessen, P. Hanappe, L. Steels, Citizen noise pollution monitoring, in: dg.o '09: Proceedings of the 10th Annual International Conference on Digital Government Research – Social Networks: Making Connections between Citizens, Data and Government (Universidad de las Americas Puebla (UDLA), Puebla, Mexico; May 17-20, 2009) 390, 2009, pp. 96–103.
- [4] M. Contrafatto, J. Ferguson, D. Power, L. Stevenson, D. Collison, Understanding power-related strategies and initiatives: The case of the european commission green paper on CSR, *Account. Audit. Account.* J. 33 (3) (2020) 559–587.
- [5] T.H.E.E.C. Parliament, E. Union, Assessment and management of environmental risks, *Assess. Manag. Environ. Risks* (2001) 12–25, <https://doi.org/10.1007/978-94-010-0987-4>.
- [6] C. Cengiz, A.Ö. Boz Demir, M. Özayvuz, Evaluation of small-scale touristic coastal town by noise mapping, *Environ. Monit. Assess.* 195 (2) (2023) 335.
- [7] N. Singh, S.C. Davar, Noise pollution-sources, effects and control, *J. Human Ecol.* 16 (3) (2004) 181–187, <https://doi.org/10.1080/09709274.2004.11905735>.
- [8] M.S.M. Ali, J. Jalasabri, A.M. Sood, S. Mansor, H. Shaharuddin, S. Muhamad, Wind noise from A-pillar and side view mirror of a realistic generic car model, *DriAver*, *Int. J. Veh. Noise Vib.* 14 (1) (2018) 38–61.
- [9] K. Chaitanya, S. Shenoy, R. Jayakrishnan, A review on vehicle tyre aerodynamics, in: AIP Conference Proceedings 2317, Feb. 2021, <https://doi.org/10.1063/5.0036145>.
- [10] H. Yuan, Z. Yang, Y. Wang, Y. Fan, Y. Fang, Experimental analysis of hydrodynamic and acoustic pressure on automotive front side window, *J. Sound Vib.* 476 (March) (2020), 115296, <https://doi.org/10.1016/j.jsv.2020.115296>.
- [11] M. Hartmann, et al., Wind noise caused by the a-pillar and the side mirror flow of a generic vehicle model, in: 18th AIAA/CEAS Aeroacoustics Conference (33rd AIAA Aeroacoustics Conference), 2012, pp. 4–6.
- [12] M. Cabrol, Y. Detandt, M. Hartmann, A. Mutzke, A comparison between the effects of turbulent and acoustic wall pressure fluctuations inside a car, in: 18th AIAA/CEAS Aeroacoustics Conference (33rd AIAA Aeroacoustics Conference), 2012, pp. 4–6, <https://doi.org/10.2514/6.2012-2202>.
- [13] M. Mancinelli, T. Pagliaroli, A. di Marco, R. Camussi, T. Castelain, Wavelet decomposition of hydrodynamic and acoustic pressures in the near field of the jet, *J. Fluid Mech.* 813 (2017), <https://doi.org/10.1017/jfm.2016.869>.
- [14] H.K. Jawahar, S. Meloni, R. Camussi, Jet noise sources for chevron nozzles in under-expanded condition, *Int. J. Aeroacoust.* (2022), <https://doi.org/10.1177/1475472X221101766>.
- [15] D. Blanchet, A. Golota, N. Zerbib, L. Mebarek, Wind noise source characterization and how it can be used to predict vehicle interior noise, *SAE Tech. Pap.* 2014-June (December 2020) (2014), <https://doi.org/10.4271/2014-01-2052>.
- [16] M. Hartmann, et al., Wind noise caused by the a-pillar and the side mirror flow of a generic vehicle model, in: 18th AIAA/CEAS Aeroacoustics Conference (33rd AIAA Aeroacoustics Conference), 2012.
- [17] R.G. Dejong, T.S. Bharji, J.J. Lee, Vehicle wind noise analysis using a sea model with measured source levels, *SAE Tech. Pap.* (724) (2001), <https://doi.org/10.4271/2001-01-1629>.
- [18] P.G. Bremner, M. Zhu, Recent progress using SEA and CFD to predict interior wind noise, *SAE Int.* (2003-01-1705) (2003), <https://doi.org/10.4271/2003-01-1705>.
- [19] P.G. Bremner, J.F. Wilby, Aero-vibro-acoustics: problem statement and methods for simulation-based design solution, in: 8th AIAA/CEAS Aeroacoustics Conference and Exhibit, 2002, <https://doi.org/10.2514/6.2002-2551>.
- [20] F. Alam, S. Watkins, G. Zimmer, Mean and time-varying flow measurements on the surface of a family of idealised road vehicles, *Exp. Therm. Fluid Sci.* 27 (5) (2003) 639–654, [https://doi.org/10.1016/S0894-1777\(02\)00278-9](https://doi.org/10.1016/S0894-1777(02)00278-9).
- [21] B. Li, C.C. Ye, Z.H. Wan, N.S. Liu, D.J. Sun, X.Y. Lu, Noise control of subsonic flow past open cavities based on porous floors, *Phys. Fluids* 32 (12) (2020), <https://doi.org/10.1063/5.0028689>.
- [22] G. Nasif, R. Balachandar, R.M. Barron, Influence of bed proximity on the three-dimensional characteristics of the wake of a sharp-edged bluff body, *Phys. Fluids* 31 (2) (2019), <https://doi.org/10.1063/1.5085666>.
- [23] V.S. Yadav, N. Ganta, B. Mahato, M.K. Rajpoot, Y.G. Bhumkar, New time-marching methods for compressible Navier-Stokes equations with applications to aeroacoustics problems, *Appl. Math. Comput.* 419 (2022), 126863, <https://doi.org/10.1016/j.amc.2021.126863>.
- [24] A.M. Shinneeb, R. Balachandar, K. Zouhri, Effect of gap flow on the shallow wake of a sharp-edged bluff body - coherent structures, *Phys. Fluids* 30 (6) (2018), <https://doi.org/10.1063/1.5022252>.
- [25] T. Belamri, Y. Egorov, F. Menter, CFD simulation of the aeroacoustic noise generated by a generic side view car mirror, in: 13th AIAA/CEAS Aeroacoustics Conference (28th AIAA Aeroacoustics Conference), 2007, pp. 1–12.
- [26] M. Elgendi, M. AlMallah, A. Abdelhalig, M.Y.E. Selim, A review of wind turbines in complex terrain, *Int. J. Thermofluids* (2023), 100289.
- [27] H. Jaffar, L. Al-Sadawi, A. Khudhair, T. Biedermann, Aerodynamics improvement of DU97-W-300 wind turbine flat-back airfoil using slot-induced air jet, *Int. J. Thermofluids* 17 (2023), 100267.
- [28] Y. Wang, D. Thompson, Z. Hu, Effect of wall proximity on the flow over a cube and the implications for the noise emitted, *Phys. Fluids* 31 (7) (2019), <https://doi.org/10.1063/1.5096072>.
- [29] H.D. Yao, L. Davidson, Generation of interior cavity noise due to window vibration excited by turbulent flows past a generic side-view mirror, *Phys. Fluids* 30 (3) (2018), <https://doi.org/10.1063/1.5008611>.
- [30] J. Ask, L. Davidson, The sub-critical flow past a generic side mirror and its impact on sound generation and propagation, in: Collection of Technical Papers - 12th AIAA/CEAS Aeroacoustics Conference 3, 2006, pp. 1925–1944, <https://doi.org/10.2514/6.2006-2558>.
- [31] R. Höld, A. Brenneis, A. Eberle, V. Schwarz, R. Siegert, Numerical simulation of aeroacoustic sound generated by generic bodies placed on a plate: part I - prediction of aeroacoustic sources, in: 5th AIAA/CEAS Aeroacoustics Conference and Exhibit, May 1999, <https://doi.org/10.2514/6.1999-1896>.
- [32] R. Siegert, V. Schwarz, J. Reichenberger, Numerical simulation of aeroacoustic sound generated by generic bodies placed on a plate: part II - prediction of radiated sound pressure, in: 5th AIAA/CEAS Aeroacoustics Conference and Exhibit, May 1999, <https://doi.org/10.2514/6.1999-1895>.
- [33] T. Rung, D. Eschricht, J. Yan, F. Thiele, Sound radiation of the vortex flow past a generic side mirror, in: 8th AIAA/CEAS Aeroacoustics Conference and Exhibit, 2002, pp. 1–10, <https://doi.org/10.2514/6.2002-2549>.
- [34] Z.T. Equation, T. Models, Zonal two equation k- ϵ , turbulence models for aerodynamic flows . Florian R. Menter E lo ret Institute, Sunny vale. Mailing address : 24th fluid dynamics conference zonal two equation k - o turbulence models for aerodynamic flows, *Fluid Dyn.* (1993).
- [35] F.R. Menter, Two-equation eddy-viscosity turbulence models for engineering applications, *AIAA J.* 32 (8) (1994) 1598–1605, <https://doi.org/10.2514/3.12149>.
- [36] D.C. Wilcox, *Turbulence Modeling for CFD*, Third Edit, DCW Industries, 2006.
- [37] Y. Wang, D. Thompson, Z. Hu, Numerical investigations on the flow over cuboids with different aspect ratios and the emitted noise, *Phys. Fluids* 32 (2) (2020), <https://doi.org/10.1063/1.5131827>.
- [38] H.D. Yao, L. Davidson, L.E. Eriksson, Noise radiated by low-Reynolds number flows past a hemisphere at $Ma = 0.3$, *Phys. Fluids* 29 (7) (2017) 1–14, <https://doi.org/10.1063/1.4994592>.
- [39] B. Mahato, N. Ganta, Y.G. Bhumkar, Mitigation of aerodynamic sound for a laminar flow past a square cylinder using a pair of cowl plates, *Phys. Fluids* 32 (7) (2020), <https://doi.org/10.1063/5.0010932>.
- [40] T. Darabseh, D. Al-Yafeai, A.-H.I. Mourad, Energy harvesting from car suspension system: mathematical approach for half car model, *J. Mech. Eng. Sci.* 15 (1) (2021) 7695–7714, <https://doi.org/10.15282/jmes.15.1.2021.07.0607>.
- [41] D. Al-Yafeai, T. Darabseh, A.H.I. Mourad, Energy harvesting from car suspension system subjected to random excitation, in: 2020 Advances in Science and Engineering Technology International Conferences, ASET 2020, 2020, <https://doi.org/10.1109/ASET48392.2020.9118233>.
- [42] D. Al-Yafeai, T. Darabseh, A.H.I. Mourad, Quarter vs. half car model energy harvesting systems, in: 2019 Advances in Science and Engineering Technology International Conferences, ASET 2019, 2019, pp. 1–5, <https://doi.org/10.1109/ICASET.2019.8714433>.
- [43] D. Al-Yafeai, T. Darabseh, A.H.I. Mourad, A state-of-the-art review of car suspension-based piezoelectric energy harvesting systems, *Energies (Basel)* 13 (9) (2020), <https://doi.org/10.3390/en13092336>.
- [44] R.H. Bernard, *Road Vehicle Aerodynamic Design*, 3rd Edit, Mechaero Publishing, 2010.
- [45] S. Watkins, G. Oswald, The flow field of automobile add-ons - With particular reference to the vibration of external mirrors, *J. Wind Eng. Ind. Aerodyn.* 83 (1–3) (1999) 541–554, [https://doi.org/10.1016/S0167-6105\(99\)00100-2](https://doi.org/10.1016/S0167-6105(99)00100-2).
- [46] A.A. Lawson, D.B. Sims-Williams, R.G. Dominy, Effects of on-road turbulence on vehicle surface pressures in the a-pillar region, *SAE Tech. Pap.* 1 (1) (2008), <https://doi.org/10.4271/2008-01-0474>.
- [47] J. Ask, L. Davidson, A numerical investigation of the flow past a generic side mirror and its impact on sound generation, *J. Fluids Eng., Trans. ASME* 131 (6) (2009) 062101–06110212, <https://doi.org/10.1115/1.3129122>.
- [48] M. Zaareer, A.H. Mourad, Effect of vehicle side mirror base position on aerodynamic forces and acoustics, *Alex. Eng. J.* 61 (2) (2022), <https://doi.org/10.1016/j.aej.2021.06.049>.
- [49] M.N.M. Zaareer, "Aerodynamics and aeroacoustics optimization of vehicle's side mirror base and exhaust pipe," 2022.
- [50] J. Ask, L. Davidson, *The Near Field Acoustics of a Generic Side Mirror Based On an Incompressible Approach*, Chalmers University of Technology, 2005.
- [51] G.J. Ehlers, R.J. Chapman, R.S. Thomas, *Wind Noise and Aerodynamic Drag Optimization of Outside Rear View Mirrors*, SAE International, 2018.

- [52] G.C. Peng, Measurement of Exterior Surface Pressures and Interior Cabin Noise in Response to Vehicle Form Changes, SAE International, 2011, <https://doi.org/10.4271/2011-01-1618>.
- [53] K.K. Chode, H. Viswanathan, K. Chow, Noise emitted from a generic side-view mirror with different aspect ratios and inclinations, *Phys. Fluids* 33 (8) (2021), <https://doi.org/10.1063/5.0057166>.
- [54] J. Ye, et al., Investigation of aerodynamic noise reduction of exterior side view mirror based on bionic shark fin structure, *Appl. Acoustics* 182 (2021), 108188, <https://doi.org/10.1016/j.apacoust.2021.108188>.
- [55] H. Liu, et al., Aeroacoustic optimization of the bionic leading edge of a typical blade for performance improvement, *Machines* 9 (8) (2021), <https://doi.org/10.3390/machines9080175>.
- [56] I. Afgan, C. Moulinec, D. Laurence, Numerical simulation of generic side mirror of a car using large eddy simulation with polyhedral meshes, *Int. J. Numer. Methods Fluids* 56 (8) (2008), <https://doi.org/10.1002/fld.1719>.
- [57] J.H. Ferziger, M. Peric, A. Leonard, Computational methods for fluid dynamics table of contents, *Phys Today* 50 (3) (1997) 80.
- [58] H. Jasak, *Error Analysis and Estimation For Finite Volume Method With Applications to Fluid Flow*, University of London, 1996.
- [59] L. Yu, S. Diasinos, B. Thormber, A fast transient solver for low-Mach number aerodynamics and aeroacoustics, *Comput. Fluids* 214 (2021), 104748, <https://doi.org/10.1016/j.compfluid.2020.104748>.
- [60] H. Yuan, Z. Yang, Q. Li, Effects of installation environment on flow around rear view mirror, *SAE Int. J. Passenger Cars - Mech. Syst.* 10 (2) (2017) 580–590, <https://doi.org/10.4271/2017-01-1517>.
- [61] T. Belamri, Y. Egorov, F. Menter, CFD simulations of the aeroacoustic noise generated by a cavity flow, in: Proceedings of ASME Fluids Engineering Division Summer Meeting2006, FEDSM2006 2 FORUMS, 2006, pp. 815–824, <https://doi.org/10.1115/fedsm2006-98561>.
- [62] Y. Egorov, F. Menter, R. Lechner, D. Cokljat, The scale-adaptive simulation method for unsteady turbulent flow predictions. part 2: application to complex flows, *Flow Turbul. Combust.* 85 (2010) 139–165.
- [63] Y. Egorov, F.R. Menter, The scale-adaptive simulation method for unsteady turbulent flow predictions. part 1: theory and model description, *Flow Turbul. Combust.* 85 (1) (2010) 139–165, <https://doi.org/10.1007/s10494-010-9265-4>.
- [64] J. Wu, O. Stalnov, W. Chen, Z. Yang, X. Huang, Transient analysis of blade-vortex interaction noise, *Aerosp. Sci. Technol.* 120 (2022), 107294, <https://doi.org/10.1016/j.ast.2021.107294>.
- [65] J.E. Ffowcs Williams, D.L. Hawkings, Sound generation by turbulence and surfaces in arbitrary motion, *Philos. Trans. R. Soc. London. Series A, Math. Phys. Sci.* 264 (1151) (1969) 321–342.
- [66] J.E.F. Williams, D.L. Hawkings, Sound generation by turbulence and surfaces in arbitrary motion, *R. Soc. London-Philos. Trans. Ser. A* 264 (1151) (1969), <https://doi.org/10.1098/rsta.1969.0031>.
- [67] M. Kadivar, D. Tormey, G. McGranaghan, A review on turbulent flow over rough surfaces: fundamentals and theories, *Int. J. Thermofluids* 10 (2021), 100077.
- [68] H. Yuan, Z. Yang, Y. Wang, Y. Fan, Y. Fang, Experimental analysis of hydrodynamic and acoustic pressure on automotive front side window, *J. Sound Vib.* 476 (March 2021) (2020), 115296, <https://doi.org/10.1016/j.jsv.2020.115296>.
- [69] P.M. Rabinowitz, “The public health significance of noise-induced hearing loss,” *Noise-Induced Hearing Loss: Scientific Advances*, pp. 13–25, 2012.
- [70] S. Dong, L. Zheng, X. Zhang, P. Lin, Improved drag force model and its application in simulating nanofluid flow, *Microfluid Nanofluid* (2014), <https://doi.org/10.1007/s10404-014-1330-1>.
- [71] M. Lee, C. Ho, Lift force of delta wings, *Am. Soc. Mech. Eng.* 43 (9) (1990).
- [72] T.R. Auton, The lift force on a spherical body in a rotational flow, *J. Fluid Mech.* 183 (1987) 199–218.
- [73] T. Belamri, Y. Egorov, F. Menter, CFD simulation of the aeroacoustic noise generated by a generic side view car mirror, in: 13th AIAA/CEAS Aeroacoustics Conference (28th AIAA Aeroacoustics Conference), 2007, pp. 1–12, <https://doi.org/10.2514/6.2007-3568>.